ERJ
Engineering Research Journal
Faculty of Engineering
Minoufiya University

GEOID MODELLING FROM VERTICAL DEFLECTIONS AND GRAVITY DISTURBANCES: THE EFFECT OF CAP SIZE

Raaed M. K. Hassouna and Fahmy F. F. Asal

Department of Civil Engineering, Faculty of Engineering,
Minoufiya University, Shebin El-Kom, Egypt

ABSTRACT:

In this paper, the effect of integration cap size on geoid determination was studied, when using gravity disturbances and vertical deflection as input data. For this purpose, a series of varying cap radii was used to predict gravimetric geoidal heights at discrete GPS-Benchmarks, using both the Hotine and deflection-geoid techniques. In both cases, the results showed significant dependence of the resulting geoid accuracy on the integration cap size. The two methods showed comparable behavior in the vicinity of the cap radius, which is consistent with the maximal resolution of the reference geopotential model. At larger cap sizes, the performance of the deflection data type was significantly better than the gravity disturbances, which in turn showed a dramatic degradation of the geoid accuracy. Therefore, when solving for the geoid without modifying the integration kernel, it is strongly recommended to use large cap sizes along with the deflection-geoid method. If gravity disturbances are to be used for geoid determination, then it is recommended to use as small integration cap as possible.

في هذا البحث تمت دراسة تأثير نصف قطر نطاق التكامل على حساب الجيوئيد، وذلك في حالة استخدام اضطراب الجاذبية وانحراف الرأسي عن العمودي كبيانات مدخلة. ولهذا الغرض تم أخذ قيم متعددة لنصف قطر نطاق التكامل لتعيين الجيوئيد عند نقط (GPS) متفرقة ومعلومة المنسوب، وذلك باستخدام طريقتي (Hotine) و (Deflection-geoid). وقد أظهرت النتائج في كلتا الحالتين تأثيرا ملحوظا لنصف قطر نطاق البيانات على دقة الجيوئيد. وقد أعطت الطريقتان نتائج متشابهة عند نصف القطر المتوافق مع تحليل النموذج التوافقي المستخدم. ولكن عند أقطار أكبر لنطاق البيانات اتضح أن دقة الطريقة الأولى تتدهور، بينما كانت نتائج الطريقة الثانية أفضل بشكل ملحوظ. لذا يوصى باستخدام أقل قطر ممكن لنطاق البيانات في حالة استخدام أرصاد اضطراب الجاذبية في حساب الجيوئيد، بينما يوصى باستخدام قيم أكبر في حالة استخدام أرصاد انحراف الرأسي عن العمودي، وذلك في حالة عدم إجراء أي تعديل على دالة التكامل أثناء الحل.

Keywords: Ceoid - cap size - gravity - deflection

1. INTRODUCTION

Gravimetric geoid determination via the model approach is generally characterized by solving the geodetic boundary value problem (GBVP) using integral formulas. In modern geoid determination, the integration is carried out over a limited integration cap around the computational point. Such cap is supposed to provide the effect of local data, giving the medium-to-short wavelength component of the gravimetrically predicted geoidal height. The long wavelength spectrum is synthesized from an appropriate high-resolution geopotential model, whereas the high frequency features are implied by the topographic effect in the vicinity of the computation point.

Theoretically, the integration cap radius ψ_0 should be consistent with the maximum resolution, N_{max}, of the used geopotential model [6],

$$\psi_0 = 180^\circ / N_{max} \qquad (1)$$

However, some factors could affect the above ideal relation. Examples are the local uncertainty of the used geopotential model, the roughness of the local gravity field, the local data type, resolution and coverage ([2] and [7]).

Some previous studies have been concerned with the effect of integration cap size on geoid determination using Stokes' formula ([1] and [3]). The aim of this study is to investigate the effect of cap size on the accuracy of geoid determination, via both the Hotine and Deflection-geoid techniques. These two methods utilize gravity disturbances and vertical deflections as input data, respectively.

2. RESIDUAL GRIDDED DATA

For this research, three sets of 2'x2' gravity disturbances, meridian and prime-vertical deflection components over the Egyptian Territory were available, relative to the WGS-84 geocentric ellipsoid. These grids represent three collocation

solutions, using the Egyptian scattered heterogeneous data as input. Each of the three data grids covers the region bounded by ($22° N \le \varphi \le 32° N$; $25° E \le \lambda \le 36° E$). The low frequency contribution was removed from the data by subtracting the values, synthesized from the (650x650) high resolution EGM96EGIT geopotential model tailored to the Egyptian Territory. This harmonic model was also reduced for the local direct and indirect Helmert's topographic effect, according to the algorithm described by [5]. As such, respective gravimetric quantities could be synthesized at the geoid level, without any violation of the harmonicity domain. The 2'x2' geopotential model derived gravity disturbances and deflection components are, respectively, evaluated by ([4] and [10])

$$\delta g_{GPM} = \left(kM/r^2\right)\sum_{n=0}^{650}(n+1)(a/r)^n \sum_{m=0}^{n}\left(\bar{C}^{*}_{nm}\cos m\lambda + \bar{S}_{nm}\sin m\lambda\right)\bar{P}_{nm}(\sin\theta) \quad (2)$$

$$\xi_{GPM} = -\left(kM/r^2\gamma\right)\sum_{n=2}^{650}(a/r)^n \sum_{m=0}^{n}\left(\bar{C}^{*}_{nm}\cos m\lambda + \bar{S}_{nm}\sin m\lambda\right)d\bar{P}_{nm}(\sin\theta)/d\theta \quad (3)$$

$$\eta_{GPM} = -\left(kM/r^2\gamma\cos\theta\right)\sum_{n=2}^{650}(a/r)^n \sum_{m=0}^{n} m\left(\bar{C}^{*}_{nm}(-\sin m\lambda) + \bar{S}_{nm}\cos m\lambda\right)\bar{P}_{nm}(\sin\theta) \quad (4)$$

With:

- Θ the geocentric latitude,
- Λ the geodetic longitude,
- r the geocentric radius,
- γ the normal gravity implied by the reference ellipsoid,
- kM the geocentric gravitational constant,
- a the equatorial radius,
- $\bar{C}^{*}_{nm}$ the fully normalized spherical harmonic C-coefficients of degree n and order m, reduced for the even zonal harmonics of the reference ellipsoid,
- $\bar{S}_{nm}$ the fully normalized spherical harmonic S-coefficients of degree n and order m,
- $\bar{P}_{nm}(\sin\theta)$ the fully normalized associated Legendre function of degree n and order m.

The GTOPO30 digital elevation model [11], was used to account for Helmert's topographic effects (Figure (1)). For instance, regarding gravity disturbances, Helmert's condensation effect could be approximated by the Faye reduction value [13]

$$\delta g^{h} = \left(k\rho R^2/2\right)\left(\Delta\varphi\Delta\lambda\cos\varphi_q\right)\sum\left(\left(H_q - H_p\right)^2/l^3\right) \quad (5)$$

where

- l the distance between the computation point and the running point,
- k the gravitational constant,
- H_p the orthometric height of the computation point,
- H_q the orthometric height of the running point,
- P the mean crustal density ($\rho \approx 2.67$ gm/cm^3).

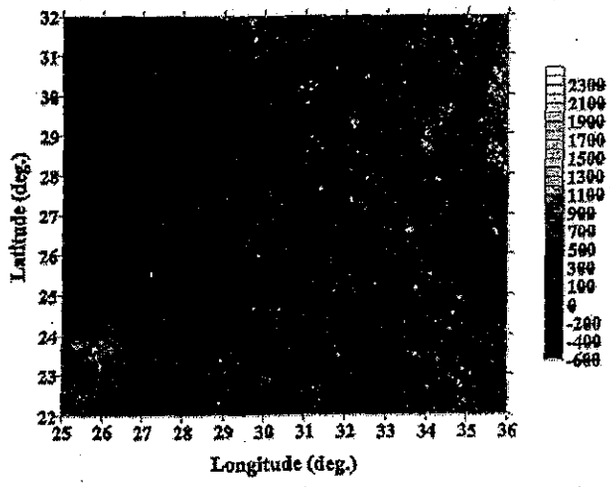

Figure (1): GTOPO30 contour map over Egypt (Interval: 100 m)

3. SCATTERED STATION SOLUTIONS

The residual medium frequency gravity disturbances and deflection components grids are used to compute sets of residual geoidal heights at scattered and suitably distributed 15 GPS/Leveling stations. These GPS data were made available from different Egyptian data sources. The stations were selected, such that the distance between the outermost points and the region boundaries did not exceed the maximum integration cap size, as shown in Figure (2). The discrete solutions were accomplished using the Hotine and Deflection-geoid formulas, respectively, where the integrations were carried out over limited caps around the discrete computational points.

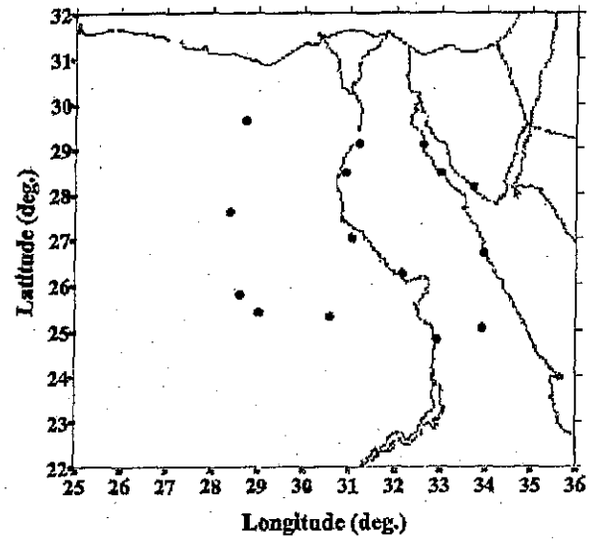

Figure (2) Distribution of the computational points.

In spherical approximation, the residual geoidal solution by Hotine's formula is expressed as [8]

$$N_p^r = (R/4\pi\gamma_p)\sum_{\varphi}\sum_{\lambda}\delta g_q^r H(\psi_{pq})\cos\varphi_q \Delta\lambda \quad (6)$$

where

R the mean radius of the Earth (taken ≈ 6371 km),

γ_p the normal gravity pertaining to p, on the WGS-84 ellipsoid,

δg_q^r the residual gravity disturbance at the running point q,

$\Delta\varphi$ & $\Delta\lambda$ the data grid spacing in radians,

ψ_{pq} the spherical distance between p and q, expressed as

$$\cos\psi_{pq} = \sin\varphi_p \sin\varphi_q + \cos\varphi_p \cos\varphi_q \cos(\lambda_q - \lambda_p) \quad (7)$$

$H(\psi)$ is the Hotine's kernel, expressed by;

$$H(\psi) = 1/\sin(\psi/2) - \ln[1 + 1/\sin(\psi/2)] \quad (8)$$

On the other hand, the residual geoid undulation is formulated by the Deflection-geoid technique, as follows;

$$N_p^r = (R/4\pi)\sum_{\varphi}\sum_{\lambda}(\xi_q^r \cos\alpha_{qp} + \eta_q^r \sin\alpha_{qp}).$$
$$dC(\psi_{pq})/d\psi_{pq}.\cos\varphi_q\ \Delta\varphi\ \Delta\lambda \quad (9)$$

where ξ^r_q & η^r_q are the residual meridian and prime-vertical deflection components, respectively, at the running point q; and α_{qp} is the azimuth of the spherical arc qp [4],

$$\tan\alpha_{qp} = (-\cos\varphi_p.\sin\Delta\lambda_{pq})/[2\sin\varphi_q.\cos\varphi_p. \sin^2(\Delta\lambda_{pq}/2) - \sin\Delta\varphi_{pq}] \quad (10)$$

$C(\psi_{pq})$ is given by

$$C(\psi) = -2\log\sin(\psi/2) - 1.5\cos(\psi) - 1 \quad (11)$$

and,

$$dC(\psi)/d\psi = -\cot(\psi/2) + 1.5\sin(\psi) \quad (12)$$

By definition, the above integrals have singularity at the computation point. Thus, the relevant effect, δN_p, of the data value at the computation point p, is accounted for in Hotine's integration as follows;

$$\delta N_p = (\delta g_p^r/\gamma_p)\sqrt{(\Delta\varphi\Delta\lambda\cos\varphi_p/\pi)} \quad (13)$$

Regarding the Deflection-geoid technique, the corresponding value is expressed as [4]

$$\delta N_p = R^2(\xi_y^r + \eta_x^r)(\Delta\varphi\Delta\lambda\cos\varphi_p/4\pi) \quad (14)$$

where ξ^r_y & η^r_x are the north and south gradients of the residual meridian and prime-vertical deflection components, respectively, at the computational point p.

The Stokes' algorithm [9] was switched into the Hotine and Deflection-geoid formulations. In the current work, various sets of residual geoidal solutions were carried out at the discrete GPS-Benchmarks, via the above two techniques, using different integration cap radii. In this respect, integration cap sizes of ψ_0 = 0.13, 0.28, 0.36, 0.5 degrees and then every 0.25° till a cap radius of 2°. The specific value ψ_0 = 0.28° corresponds to the Nyquist frequency of the reference harmonic model, according to Eq. (1). After estimating the discrete residual geoid height sets, the long and short wavelength contributions are then restored, yielding the respective full component geoidal undulation values,

$$N = N_{GPM} + N^r + N^h \quad (15)$$

The low frequency geoid was computed from the same geopotential model,

$$N_{GPM} = (kM/r\gamma)\sum_{n=0}^{650}(a/r)^n \sum_{m=0}^{n}\left(\bar{C}^*_{nm}\cos m\lambda + \bar{S}_{nm}\sin m\lambda\right)\bar{P}_{nm}(\sin\theta) \quad (16)$$

The topographic indirect effect, N^h, on the geoid is assessed as follows [13]

$$N^h = -\pi k\rho H_p^2/\gamma_p - (k\rho R^2/6\gamma_p). \sum\Delta\varphi\ \Delta\lambda\cos\varphi_q.(H_q^3 - H_p^3/l^3) \quad (17)$$

where the first term expresses the effect of the removed Bouguer plate and the second term reflects the effect of the local topographic irregularities with respect to it.

4. RESULTS

Figure (3) shows the variation of the mean difference between the GPS-derived and gravimetrically estimated geoidal heights, based on Hotine and Defection-geoid formulae; with the cap radius. The sign of the mean difference does not change. Regarding the Deflection-geoid solution, apart from a local minimum at cap radius of 0.28°, the mean difference can be considered constant till a radius of 0.75°, and then decreases with increased cap radius. In general, the Deflection-geoid method yields mean differences, which are significantly less in magnitude than those pertaining to Hotine's integral. In addition, regarding Hotine's technique, increasing the cap radius worsens the mean difference between the observed and the predicted geoidal heights. For both cases, the range of the variation of mean with cap size is about 5 cm.

Figure (4) shows a similar comparison, regarding the standard deviation (of single difference) of the discrepancies between the observed and estimated geoid undulations at the discrete GPS-Benchmarks. Just beyond a cap radius of 0.28°, the two trends

intersect, and then the Hotine method yields a monotone increase of the standard deviation as the cap radius increases, while the Deflection-geoid method shows a decreasing trend in general. Specifically, at an integration cap radius of 0.28° and less, the Hotine solution gives a little better standard deviation of difference. Moreover, at $\psi_0 = 0.28°$, the Deflection-geoid trend has a local maximum. The Hotine and Deflection-geoid methods yield a standard deviation variation range, with cap size, of about 13 and 10 cm, respectively. It should be emphasized that the resulting Hotine trends resemble those obtained from Stokes' method in [3].

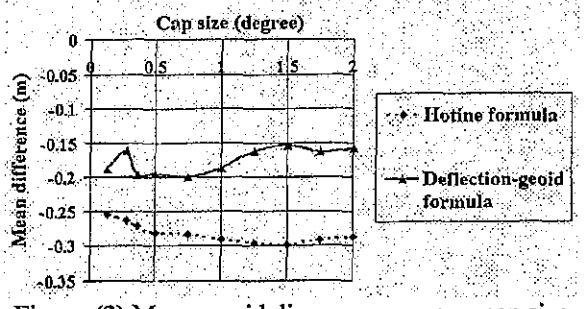

Figure (3) Mean geoid discrepancy versus cap size

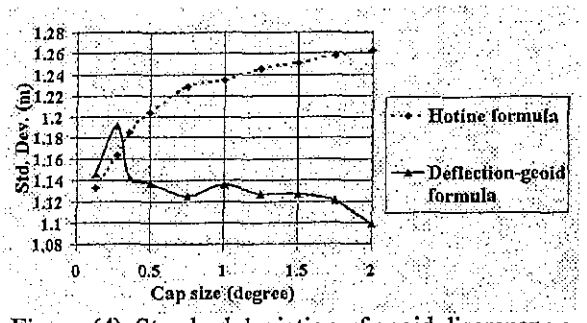

Figure (4) Standard deviation of geoid discrepancy versus cap size

5. CONCLUSIONS

In terms of the mean geoid discrepancy, the Hotine method results in a bias, which is significantly larger than that pertaining to the Deflection-geoid method. This bias exhibits a nearly monotone increase, as the integration cap size increases. Beside at an integration cap consistent with the harmonic model's resolution ($\psi_0 = 0.28°$), the Deflection-geoid method is still capable of reproducing a quite small value for the mean difference at large cap radii. Regarding the standard deviation of difference, the two gravity disturbance and vertical deflection data types yield comparable features in the vicinity of $\psi_0 = 0.28°$. This implies that the reference geopotential model is consistent with the local data. Slightly exceeding that cap size value, the corresponding trends diverge dramatically, where the vertical deflection data type shows significantly better standard deviations. At a cap size of 2°, the standard deviation pertaining to the Deflection-geoid solution becomes better than that of the Hotine method by about 16 cm.

Due to its relatively rough nature [2], the gravity disturbance data seems to work well only within a limited integration cap that describes its high frequency nature. Being the horizontal gradient of the geoid, the vertical deflections have moderate spatial variability, and hence they may give better results with larger cap sizes. Moreover, such different behaviours could be also attributed to the lack of modification of the integration kernels in both solutions [12]. In particular, the unmodified Hotine's kernel could have adversely degraded the solution, when using larger cap sizes.

Based on the obtained results, and when solving for the geoid without modifying the integration kernel, it is recommended to use a large cap size along with the Deflection-geoid technique. This would provide the best results. If gravity disturbance data are to be used, then the smallest possible integration cap radius should be used. Also, the application of modified kernels to both the Hotine and Deflection-geoid techniques should be investigated, whether it would yield consistent geoidal height accuracies.

6. REFERENCES

[1] Forsberg, R and W.E. Featherstone, (1998): "Geoids and Cap Sizes", *in: Geodesy on the Move: Gravity, Geoids, Geodynamics and Antarctica*", Forsberg, R., Feissel, M. and Dietrich, R. (eds.), Springer, Berlin, Germany, pp: 194-200.

[2] Groten, E. (1981): "Local and Global Gravity Field Representation", *Reviews of Geophysics and Space Physics"*, Vol. 19, No. 2, August, pp: 407-414.

[3] Higgins, M.B., R. Forsberg and A.H.W. Kearsley (1997): "The Effects of Varying Cap Sizes on Geoid Computations: Experiences with FFT and Ring Integration", *Paper presented at the IAG Scientific Assembly*, Rio de Janeiro, September.

[4] Hwang, C. (1998): "Inverse Vening Meinesz formula and Deflection-geoid formula: applications to the predictions of gravity and geoid over the South China Sea", *Journal of Geodesy*, 72, pp: 304-312.

[5] Nahavandchi, H. and L.E. Sjöberg (1998): "Terrain corrections to power H^3 in gravimetric geoid determination", *Journal of Geodesy*, 72, pp: 124-135.

[6] Rapp, R.H. (1977): "The relationship between mean anomaly block sizes and spherical harmonic representations", *Journal of Geophysical Research*, Vol. 82, No. 33, pp: 5360-5364.

[7] Rapp, R.H. (1998): "Past And Future Developments In Geopotential Modeling", *Geodesy on the Move*, Forsberg, Feissel, Dietrich (eds), Springer-Verlag, Berlin New York, pp: 58-78.

[8] Serpas, J.G. (2003): "Local and Regional Geoid Determination from Vector Airborne Gravimetry", *Report No. 468, Department of Civil and Environmental Engineering and Geodetic Science,* The Ohio State University.

[9] Tscherning, C.C., R. Forsberg, and P. Knudsen (1992): "The GRAVSOFT Package for Geoid Determination", *Press. 1. Continental Workshop on the European Geoid*, Prague, May.

[10] Tscherning, C.C., R.H. Rapp and C. Goad (1983): "A Comparison of Methods for Computing Gravimetric Quantities from High Degree Spherical Harmonic Expansions", manuscripta geodetica, Vol. 8: 249-272.

[11] USGS (2000): "GTOPO30", *http://www.cr.usgs. gov/ glis/hyper/guide/gtopo30.*

[12] Vaníček, P. and W.E. Featherstone (1998): "Performance of three types of Stokes's kernel in the combined solution for the geoid", Journal of Geodesy, 72: 684-697.

[13] Véronneau, M. (1996): "The GSD95 Geoid Model for Canada", *Proceedings of the International Symposium on Gravity, Geoid and Marine Geodesy (GRAGEOMAR 1996)*, Tokyo, September 30 to October 5.